ROYAL SOCIETY
OF CHEMISTRY

PAPER

Check for updates

Improved charge storage performance of a layered Mo$_{1.33}$C MXene/MoS$_2$/graphene nanocomposite†

Ahmed EL Ghazaly, [ID] [a] Ulises A. Méndez-Romero,[b] Joseph Halim, [ID] [a] Eric Nestor Tseng,[c] Per O. Å. Person, [ID] [c] Bilal Ahmed,[c] Ergang Wang [ID] [b] and Johanna Rosen*[a]

The construction of nanocomposite electrodes based on 2D materials is an efficient route for property enrichment and for exploitation of constituent 2D materials. Herein, a flexible Mo$_{1.33}$C *i*-MXene/MoS$_2$/ graphene (MOMG) composite electrode is constructed, utilizing an environment-friendly method for high-quality graphene and MoS$_2$ synthesis. The presence of graphene and MoS$_2$ between MXene sheets limits the commonly observed restacking, increases the interlayer spacing, and facilitates the ionic and electronic conduction. The as-prepared MOMG electrode delivers a volumetric capacitance of 1600 F cm^{-3} (450 F g^{-1}) at the scan rate of 2 mV s^{-1} and retains 96% of the initial capacitance after 15 000 charge/discharge cycles (10 A g^{-1}). The current work demonstrates that the construction of nanocomposite electrodes is a promising route towards property enhancement for energy storage applications.

1. Introduction

Two-dimensional (2D) materials have garnered widespread research attention for a wide array of applications due to their unique electrical, thermal, mechanical, and optical properties.[1,2] The strong covalent bond structure such as in MoS$_2$ and graphene, as well as rich chemistry, motivates nanoscale engineering researchers to manipulate the 2D layers by doping, alloying or layer mixing. In addition to the high specific surface area, the layered structure becomes an efficient transportation route for electron and ions, facilitating the charge transport and reducing the ionic diffusion length in aqueous electrolytes.[3]

Recently, a family of 2D transition metal carbides/nitrides, MXenes,[4–6] have shown potential in the field of electromagnetic shielding,[7] high speed antennas,[8] printed electronics,[9]- field emitters[10] and energy storage devices,[11,12] including secondary-ion batteries,[13,14] and supercapacitors.[15] MXenes are produced by selective chemical etching of the parent MAX phases,[16] which are ternary transition metal carbides, nitrides or carbonitrides with a generic formula of M$_{n+1}$AX$_n$, where n is an integer (1, 2 and 3), M refers to a transition metal element, A represents the A-group element (mainly Al or Si), and X denotes carbon and/or nitrogen.

In 2017, quaternary *i*-MAX phases,[17–19] such as (Mo$_{2/3}$Sc$_{1/3}$)$_2$AlC, with in-plane chemical ordering of the two M elements, were reported.[17] Similar to conventional MAX phases, the selective etching of aluminum (Al) from the parent *i*-MAX phase realizes 2D sheets, whereas additional removal of scandium (Sc) results into the formation of MXene with ordered vacancies, referred to as *i*-MXene. The first reported member of the *i*-MXene family, *i.e.*, Mo$_{1.33}$C, can form high-density films (3.7 g cm^{-3}) and render a high volumetric capacitance of ~1150 F cm^{-3} in 1 M H$_2$SO$_4$.[17] This number has been increased to ~1600 F cm^{-3} by post treatment procedures.[20] Even though the as-prepared *i*-MXenes deliver higher capacitance than conventional as-prepared MXenes, this family faces similar challenges like other laminar structure materials.[21] For instance, the restacking occurs between MXene sheets during electrode filtration, which should be avoided to obtain optimal supercapacitive performance. One should note that the stacked sheets limit the ionic intercalation and negatively influence the electrochemical performance.

To avoid the restacking of MXene electrodes, they can be reinforced with other additive materials. For instance, MXene can be mixed with electrochemically active polymers, such as PEDOT:PSS,[22] cellulose,[23] PVA[24] and PANI,[25] to minimize restacking and obtain high capacitance, superior stability and desirable film flexibility. Previously, MXene-based 2D composites have exhibited improved electrochemical storage properties, *e.g.*, pristine Ti$_3$C$_2$ MXene delivers a volumetric capacitance of 700 F cm^{-3} while a Ti$_3$C$_2$/graphene composite delivers a higher volumetric capacitance of 1040 F cm^{-3}.[26] However, the decreased film density due to the presence of additive materials compromises the volumetric capacitance. For example, adding materials to Ti$_3$C$_2$ MXene electrode with ratio of 10 wt% such as

aMaterials Design Division, Department of Physics, Chemistry and Biology (IFM), Linköping University, 581 83 Linköping, Sweden. E-mail: johanna,rosen@liu.se

bDepartment of Chemistry and Chemical Engineering, Chalmers University of Technology, Goteborg, SE-412 96 Sweden

cThin Film Physics Division, Department of Physics, Chemistry and Biology (IFM), Linköping University, 581 83 Linköping, Sweden

graphene,[27] CNT[28] and PVA[24] reduced the electrode packing density up to 30% compared to the pristine density.

Molybdenum disulfide (MoS_2) is another low cost promising candidate to improve the properties of MXene with maintaining the electrode packing density.[29] There are few reports where MoS_2 has been combined with Ti_3C_2 MXene to enhance the catalytic and Li-storage performance *via* confining MoS_2 between MXene sheets to avoid restacking and therefore increases the electrode charging capacity.[30] However, most of these reports adopt a hydrothermal process and require high synthesis temperatures for *in situ* growth of MoS_2 nanosheets on the MXene surface, which inevitably, partially oxidizes the MXene structure. Therefore, a room-temperature synthesis route, realized by physical mixing of 2D MoS_2 and MXene nanosheets, is of utmost importance to improve the electrochemical performance without any chemical reaction while retain the original structure and physical properties of the MXene.[29,31,32]

Herein, we combine an *i*-MXene, $Mo_{1.33}C$, with MoS_2 and graphene nanosheets to construct a layered $Mo_{1.33}C/MoS_2$/graphene (MOMG) nanocomposite for charge storage applications. The MoS_2 and graphene were synthesized by a top-down environment-friendly approach (*i.e.*, *n*-BuLi chemical free) using ultrasonication-assisted liquid-phase exfoliation. Structural analysis confirmed the formation of a sandwich-like MOMG film with high flexibility and pronounced interlayer distance. The solution-processable $Mo_{1.33}C/MoS_2$/graphene nanocomposite films are employed as flexible free-standing electrodes, delivering a high volumetric capacitance of 1600 F cm^{-3} at the scan rate of 2 mV s^{-1} and retaining 96% of the initial capacitance after 15 000 charge/discharge cycles. The current work demonstrates that the electrochemical performance of *i*-MXenes can be significantly enhanced by fabricating nanocomposite electrodes, indicating potential utilization of *i*-MXenes combined with other materials for energy storage applications and beyond.

2. Experimental procedure

2.1 MAX and MXene synthesis

The preparation of the *i*-MAX phase is detailed elsewhere.[17] To obtain the desired *i*-MXene, 2 g of the parent *i*-MAX powder was immersed in 20 mL of hydrofluoric acid (HF) to selectively etch-out Al and Sc, followed by stirring for 24 h at room temperature. The resulting suspension was washed with 1 M HCl for three times to remove ScF_3 and washed with distilled water several times until the pH reached ~5. To delaminate the multilayered MXene sheets, 10 mL of TBAOH (Sigma Aldrich) was mixed with MXene *via* stirring for 1 h and washed with distilled water. The MXene suspension was sonicated for 1 h under N_2 flow to obtain delaminated MXene sheets. Finally, single flakes of suspended MXene were collected after centrifugation for 1 h at 3000 rpm. The MXene suspension had a concentration of 0.6–1 mg mL^{-1}.

2.2 $Mo_{1.33}C$ nanocomposite electrode

Both graphene (G) and MoS_2 were purchased from 123dnanotech (Sweden), where the materials are synthesized by an *n*-BuLi chemical-free method using ultrasonication-assisted liquid-phase exfoliation. 50 mg of both G and MoS_2 were dry mixed in the weight ratio of 1 : 1 and dispersed in absolute ethanol. Characterization of the as-synthesized MoS_2 and graphene with respect to the structure, microstructure, and composition is included in the ESI, Fig. S4–S7.† The MoS_2/G mixture concentration was 2 g mL^{-1}. $Mo_{1.33}C$ composite electrode was prepared by mixing MoS_2/G mixture (10 wt%) with $Mo_{1.33}C$ in the solution phase, followed by gentle shaking for 10 min. The resulting suspension was vacuum filtered to obtain a flexible film (~3 μm), which was used as an electrode for electrochemical analysis.

2.3 Materials characterization

The microstructure and morphology of delaminated *i*-MXene, MoS_2, graphene flakes and free-standing electrodes were investigated by scanning electron microscope (ZEISS, LEO 1550) and scanning transmission electron microscopy (STEM) together with energy dispersive X-ray spectroscopy (EDX) using the Linköping double corrected FEI Titan³ 60–300, operated at 300 kV.[33] The crystallographic and phase analyses were performed using X-ray diffraction (XRD, Rigaku X-ray diffractometer, Cu Kα source, $2\theta = 3$–$80°$). X-ray photoelectron spectroscopy (XPS, Kratos AXIS Ultra^{DLD}, Manchester, U.K.) was used for compositional analysis, equipped with monochromatic Al Kα (1486.6 eV) source. The X-ray beam irradiated the sample surface at an angle of 45°, with respect to the surface, and provided an X-ray spot of 300 × 800 μm. The charge neutralization was performed using a co-axial, low energy (~0.1 eV) electron flood source to avoid shifts in recorded binding energy (BE). The XPS survey spectra were recorded using an analyzer pass energy of 160 eV with a step size of 0.5 eV, whereas the high-resolution S 2p spectra were recorded using an analyzer pass energy of 20 eV, in a given range, with a step size of 0.1 eV. The BE scale of all XPS spectra was referenced to the Fermi-edge (EF), which was set to a BE of 0 eV.

2.4 Electrochemical characterization

The electrochemical measurements were collected using a three-electrode plastic Swagelok cell loaded with 1 M H_2SO_4 electrolyte. An electrochemical workstation (Biological VPS) was used to record electrochemical data. In three-electrode configuration, glassy carbon, activated carbon (PTFE 7 wt%) and Ag/AgCl electrodes were employed as current collector, counter, and reference electrodes, respectively. The 4 different working electrodes tested were pure $Mo_{1.33}C$, MOMG, $Mo_{1.33}C$/graphene (5 wt%), and $Mo_{1.33}C/MoS_2$ (5 wt%). The film thickness and mass loading were ~3 μm and ~0.85 mg cm^{-2}, respectively. Also, thick MOMG films (8 μm) were prepared for high mass loading measurements. The cyclic voltammetry (CV) and galvanostatic charge/discharge curves were recorded at different scan rates and current densities, respectively. The

electrochemical impedance spectroscopy (EIS) was measured at OCV by applying a sinusoidal voltage of 5 mV in the frequency range of 10 mHz to 100 kHz.

3. Results and discussion

Fig. 1a illustrates the synthesis process of a MOMG composite film. Initially, the graphene flakes and MoS_2 (1 : 1 wt%) are dispersed in ethanol and sonicated for 10 min to avoid agglomeration of nanosheets. Then, the colloidal solution was mixed with 20 mL of MXene and handshaken for 10 min. Finally, the MOMG film was obtained by vacuum-assisted filtration. Fig. 1b shows a photo of the filtered film, exhibiting excellent flexibility due to the presence of graphene. Also, the highly oriented laminar sheets of MOMG can be observed in the cross-sectional SEM image (Fig. 1c). Fig. 1d shows XRD patterns of $(Mo_{2/3}{}^1Sc_{1/3}{}^1)_2AlC$ i-MAX powder, $Mo_{1.33}C$ i-MXene, and MOMG nanocomposite. The formation of $Mo_{1.33}C$ i-MXene is confirmed by X-ray diffraction (XRD), and the presence of a (002) MXene peak ($2\theta = 6.1°$) and absence of the parent i-MAX phase peaks.[17] Furthermore, the XRD pattern of the MOMG film shows MoS_2 peaks at 14.2°, 44° and 59°, which can be attributed

to the (002), (103) and (110) planes, respectively (JCPDS card no. 77–1716). The diffraction peak at $2\theta = 26.3°$ corresponds to the (002) diffraction planes of graphene. A significant shift in the (002) diffraction peak of MXene is observed after adding MoS_2 and graphene, which corresponds to an increase in the d spacing. A similar shift in the (002) diffraction peak has been observed in the case of Ti_3C_2 MXene, which may be ascribed to surface modification and interactions between surface functional groups and the MXene.[34]

Also, a similar increase in d-spacing by 0.35 Å and 0.45 Å are realized after the addition of 5 wt% graphene or 5 wt% MoS_2 to the MXene sheets, which may be beneficial for the charge storage performance (Fig. S1†). The high-resolution S 2p XPS spectra confirm the presence of sulfur (S 2p peak) in the MOMG film, see Fig. S2.† For further structural investigation, a cross-sectional area of the MOMG film was prepared using traditional ion-milling for STEM-EDX imaging and analysis. Fig. 1e presents a STEM image, where MXene, MoS_2 and graphene regions can be identified from the corresponding EDS elemental maps. The elemental analysis demonstrates that the three regions are separated between MoS_2, graphene and MXene, which is consistent with the XRD pattern of the MOMG
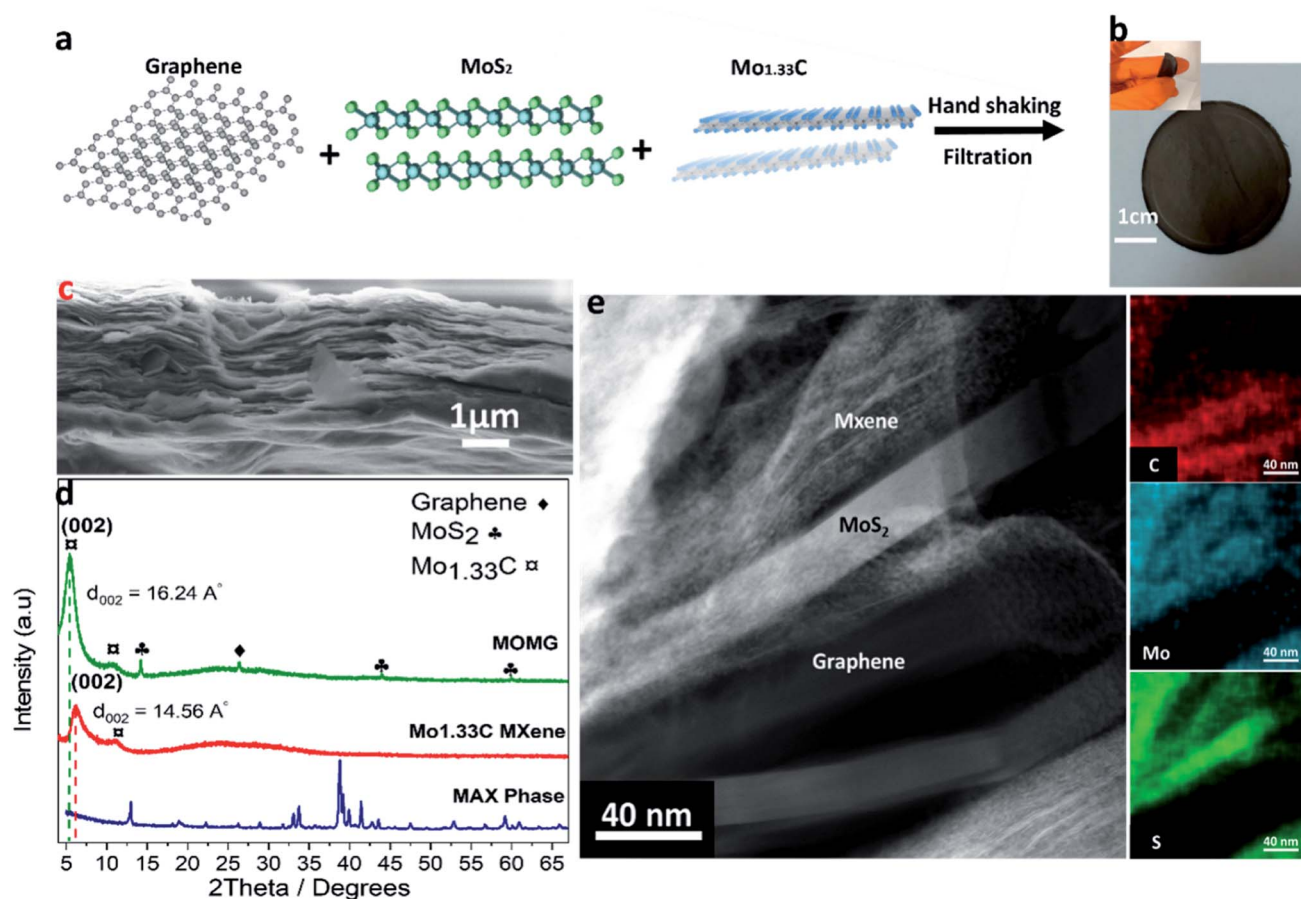

Fig. 1 (a) Schematic illustration of the structure of MXene, graphene and MoS_2, and composite synthesis steps; (b) the digital photograph of the free-standing film, showing excellent flexibility; (c) cross-sectional SEM image of the MOMG nanocomposite film, demonstrating layered structure and average thickness of 3 μm; (d) XRD patterns of $(Mo_{2/3}{}^1Sc_{1/3}{}^1)_2AlC$ i-MAX phase, $Mo_{1.33}C$ i-MXene and MOMG nanocomposite; and (e) STEM image of the cross-sectional area of MOMG film (left) with corresponding EDS elemental analysis maps (right).

film. Still, the electrode architecture opens a path for electrons to smoothly transfer between layers which clearly reflects on the electrochemical performance of the 2D composite film (see Electrochemical section). The atomic ratios of Mo, S and C from different regions, as marked in Fig. 1e, are presented in Table S1,† showing distinct differences in relative content of these elements in different regions. Hence, graphene and MoS_2 are incorporated into the MOMG composite. Furthermore, the presence of graphene has, as expected, improved the mechanical properties and conductivity of the MOMG film. The presence of MoS_2 has maintained a high packing density of the MOMG electrodes (3.55 g cm^{-3}) due to the high density of MoS_2 (~5 g cm^{-3}).

Earlier, we have demonstrated that the pristine $Mo_{1.33}C$ i-MXene has a voltage window of $+0.3$ to -0.35 V (vs. Ag/AgCl).[17] The CV profile has been reproduced in Fig. 2a, cell 2, and compared to the cell 1 setup (Fig. 2c), where glassy carbon is employed as a current collector instead of stainless steel. As shown in Fig. 2a, the CV profile (cell 1) exhibits a typical pseudocapacitive behavior within a potential window of |0.75 V|. The increase in voltage window towards the negative side is related to the suppression of hydrogen evolution reaction (HER) by the glassy-carbon current collector. A reversible couple of anodic and cathodic peaks was observed at -0.32 V and 0.15 V (vs. Ag/AgCl), respectively, revealing the pseudocapacitive behavior of $Mo_{1.33}C$ MXene. The as-prepared $Mo_{1.33}C$ MXene film delivered a volumetric capacitance of ~825 F cm^{-3} at 2 mV s^{-1}. Furthermore, the galvanostatic charge/discharge plots in Fig. 2b, at different current densities (1, 3, 5 and 10 A g^{-1}), show a symmetric triangular shape, which indicates the high

coulombic efficiency, high reversibility, and minimal IR drop. One should note that the shape of the CV curves is retained at the higher scan rates as well (2–1000 mV s^{-1}). The (inset plot in Fig. 2e) presents log I vs. log v curves at different potentials. The b-value can be obtained from the slope of the plot and indicates the charge storage mechanism. The b-value of 0.5 indicates a diffusion-controlled mechanism, whereas the b-value of 1 corresponds to a purely surface-controlled charge storage process. Herein, the b-value at different potentials ranged from ~0.7 to 1, indicating a combination of diffusion- and surface-controlled processes. It can be inferred that the utilization of glassy carbon as a current collector, did not alter the charge storage mechanism of $Mo_{1.33}C$ i-MXene, however, it did extend the voltage window by suppressing the hydrogen evolution reaction.[20]

Hence, the electrochemical performance of the MOMG composite was assessed using three-electrode setup with glassy carbon as a current collector. Fig. 3a presents the CV curves of MOMG MXene at different scan rates (2–500 mV s^{-1}) in the voltage range of -0.5 to $+0.3$ V (vs. Ag/AgCl). Despite the addition of MoS_2 that has pseudocapacitive intercalation nature in H_2SO_4 electrolyte we have not observed any additional anodic or cathodic peaks in the MOMG CV profiles indicating that the MXene electrochemical charge storage behavior still the dominant mechanism.[27,35,36] However, the MoS_2 can still improve the gravimetric capacitance by preventing the restacking of MXene sheets and contribute to ion intercalation process without any chemical reactions. The overall increase in charge storage performance may be ascribed to the enlarged of d-spacing by preventing the restacking leading to reversible (de)intercalation
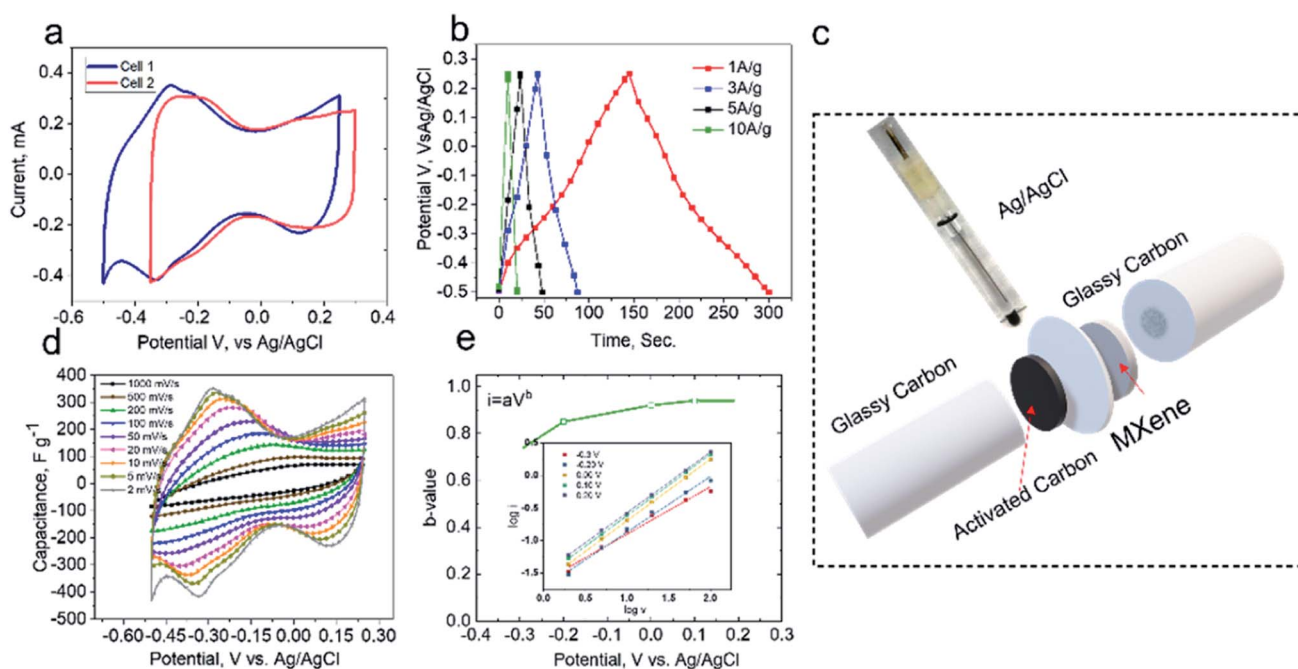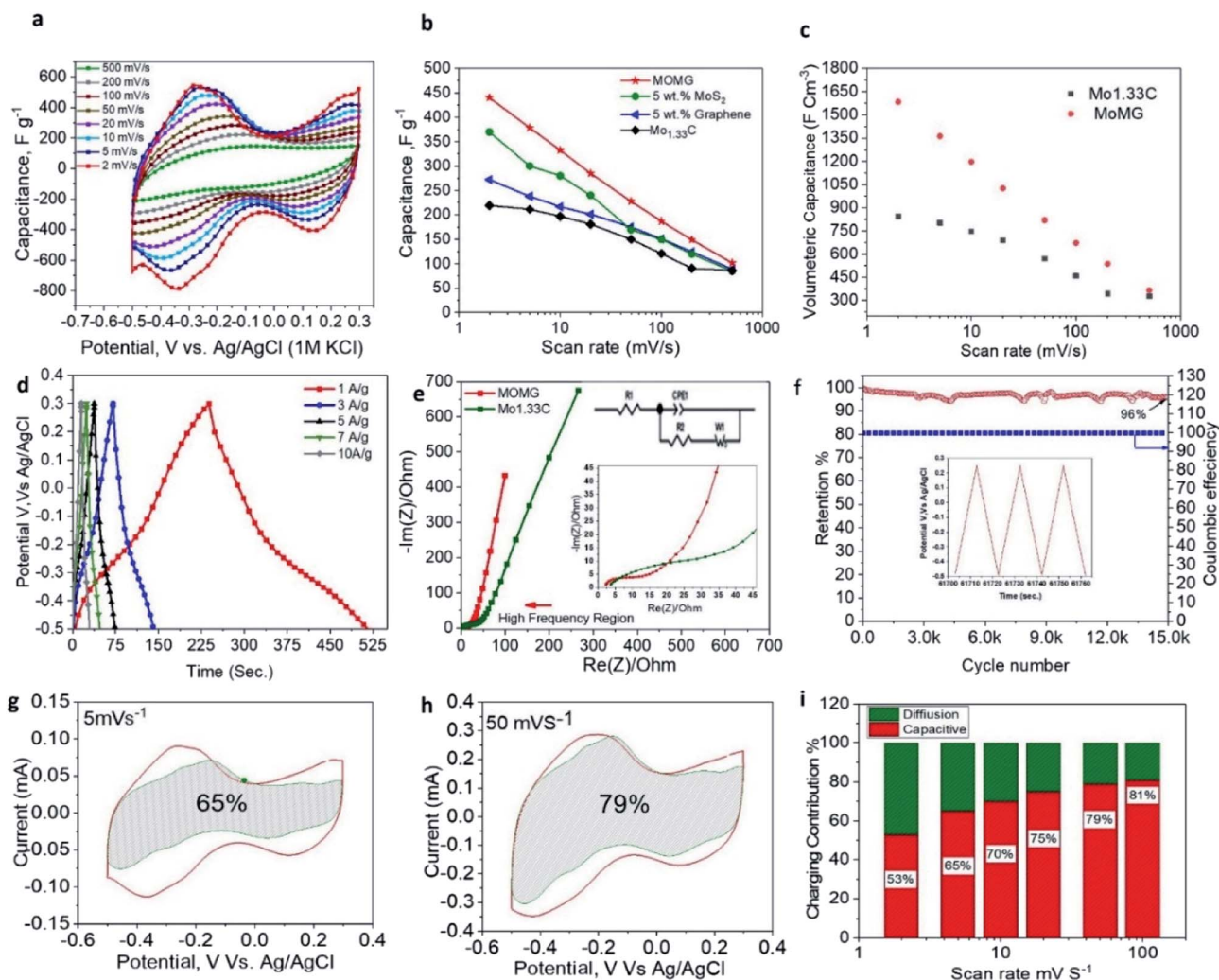

Fig. 2 (a) CV curves of $Mo_{1.33}C$ MXene at 20 mV s^{-1} using stainless steel (cell 1) and glass carbon (cell 2) as current collectors, respectively; (b) charge/discharge and (d) CV curves of $Mo_{1.33}C$ MXene at different current densities and scan rates; and (c) schematic illustration of the three-electrode setup; and (e) b-values at different potentials ($i = av^b$).

Fig. 3 (a) CV curves of MOMG electrode at different scan rates; (b and c) gravimetric and volumetric capacitances of $Mo_{1.33}C$ and $Mo_{1.33}C$-based composites, (d) charge/discharge curves at different current densities; (e) Nyquist plots of MOMG and $Mo_{1.33}C$ MXene, where the inset shows the high-frequency region and equivalent circuit; (f) cyclic stability and coulombic efficiency of MOMG electrode at 10 A g^{-1}; (g and h) relative contributions of diffusion- and surface-controlled (dark region) processes at 5 and 50 mV s^{-1} scan rate; and (i) contributions of different charge storage processes at different scan rates.

of cations and efficient transfer of electrons during the charge/discharge process.[26] It is worth emphasizing that the presence of both graphene and MoS$_2$ is required to obtain optimal electrochemical performance while maintaining the high packing density of the electrode. For instance, at the scan rate of 2 mV s^{-1}, MXene/MoS$_2$ and MXene/graphene electrodes delivered a gravimetric capacitance of 365 F g^{-1} and 270 F g^{-1}, respectively, whereas the MOMG delivered the highest gravimetric capacitance of 450 F g^{-1} (Fig. 3b).

Furthermore, as shown in Fig. S3,† similar to the MOMG nanocomposite, the $Mo_{1.33}C/MoS_2$, $Mo_{1.33}C/graphene$ and the MOMG with higher mass loading (1.8 mg cm^2) electrodes also exhibit the same CV shape and voltage window. The volumetric capacitance of $Mo_{1.33}C$ MXene and MOMG is compared in Fig. 3c, showing an increase of 94% at the scan rate of 2 mV s^{-1}. One should note that the capacitance is mainly contributed from the pseudocapacitance, and that the presence of redox peaks even at higher scan rates 50 mV s^{-1} reflects the fast cation

intercalation combined with the faradaic reactions. The charge/discharge curves of MOMG electrode were measured at the current density of 1, 3, 5, 7 and 10 A g^{-1} (Fig. 3d), confirming the high reversibility of redox reactions.

Furthermore, the electrochemical impedance spectroscopy (EIS) was employed to assess the charge transfer resistance. Fig. 3e shows the Nyquist plots of the MOMG nanocomposites and pristine MXene electrodes, revealing that the R_{ct} of the former is significantly lower than the latter, which is highly beneficial for superior electrochemical performance. It should be noted that the graphene forms a conductive network and facilitates electronic and ionic transfer, minimizing the overall ionic resistance. Moreover, Fig. 3f shows that the as-prepared MOMG electrode retains 96% of the initial capacitance after 15 000 charge/discharge cycles at the current density of 10 A g^{-1}. The superior cyclic stability can be ascribed to the structural stability of the nanocomposite electrode and absence of any undesirable reactions at the electrode/electrolyte

interface. It is worth highlighting that the as-prepared $Mo_{1.33}C$ *i*-MXene film retained 85% of the initial capacitance, whereas the $Mo_{1.33}C$/PEDOT:PSS composite retained 93% of the initial capacitance after 10 000 charge/discharge cycles in lower operating voltage windows using sulfuric acid electrolyte.[17,22] Hence, in addition to the enhanced charge storage performance, the incorporation of graphene and MoS_2 enhanced the cyclic stability of MXene-based MOMG electrodes.

MXene-based electrodes exhibit a combination of surface- and diffusion-controlled capacitive contributions. Herein, for the MOMG nanocomposite, the capacitive contribution increases from 53% to 81% with increasing scan rate from 2 mV s^{-1} to 100 mV s^{-1}, respectively suggesting a high fast charge storage at higher scan rates (Fig. 3g–i). The capacitive controlled contribution is slightly improved by 12% compared to the $Mo_{1.33}C$ reported at the same scan rate, indicating the improvement in the electrode conductivity and less charge diffusion path during ion intercalation.[17] Overall, the as-prepared nanocomposite electrodes exhibited enhanced *d*-spacing, improving ionic intercalation (accessibility) between sheets,[26] and high conductivity due to presence of graphene sheets.[27] Hence, the resulting MOMG film delivered promising results for supercapacitors.

4. Conclusions

In conclusion, we have demonstrated a solution processable method to prepare a nanocomposite material of $Mo_{1.33}C$ MXene, MoS_2 and graphene, resulting in flexible free-standing electrodes with enhanced interlayer spacing and conductivity. The results revealed that both graphene and MoS_2 have been successfully confined between MXene sheets, limiting the restacking and forming a conductive network for efficient electronic and ionic conduction. Furthermore, the MOMG film, as a supercapacitor electrode, rendered a high volumetric capacitance of 1600 F cm^{-3} at the scan rate of 2 mV s^{-1} and retained 96% of the initial capacitance after 15 000 charge/discharge cycles. These preliminary results indicate that the energy storage performance of MXene-based electrodes can be tuned by designing nanocomposites based on combinations with other materials.

Conflicts of interest

The authors declare no competing interests.

Acknowledgements

References

1 K. Khan, A. K. Tareen, M. Aslam, R. Wang, Y. Zhang, A. Mahmood, Z. Ouyang, H. Zhang and Z. Guo, *J. Mater. Chem. C*, 2020, **8**, 387–440.

2 Z. Hu, Z.-B. Liu and J.-G. Tian, *Chin. J. Chem.*, 2020, **38**, 981–995.

3 Z. Zhai, W. Yan, L. Dong, J. Wang, C. Chen, J. Lian, X. Wang, D. Xia and J. Zhang, *Nano Energy*, 2020, **78**, 105193.

4 M. Naguib, M. Kurtoglu, V. Presser, J. Lu, J. Niu, M. Heon, L. Hultman, Y. Gogotsi and M. W. Barsoum, *Adv. Mater.*, 2011, **23**, 4248–4253.

5 M. Naguib, O. Mashtalir, J. Carle, V. Presser, J. Lu, L. Hultman, Y. Gogotsi and M. W. Barsoum, *ACS Nano*, 2012, **6**, 1322–1331.

6 P. O. Å. Persson and J. Rosen, *Curr. Opin. Solid State Mater. Sci.*, 2019, **23**, 100774.

7 F. Shahzad, M. Alhabeb, C. B. Hatter, B. Anasori, S. Man Hong, C. M. Koo and Y. Gogotsi, *Science*, 2016, **353**, 1137.

8 A. Sarycheva, A. Polemi, Y. Liu, K. Dandekar, B. Anasori and Y. Gogotsi, *Sci. Adv.*, 2018, **4**, eaau0920.

9 C. Zhang, L. McKeon, M. P. Kremer, S.-H. Park, O. Ronan, A. Seral-Ascaso, S. Barwich, C. Ó. Coileáin, N. McEvoy, H. C. Nerl, B. Anasori, J. N. Coleman, Y. Gogotsi and V. Nicolosi, *Nat. Commun.*, 2019, **10**, 1795.

10 Y. Xin and Y.-X. Yu, *Mater. Des.*, 2017, **130**, 512–520.

11 M. Ghidiu, M. R. Lukatskaya, M.-Q. Zhao, Y. Gogotsi and M. W. Barsoum, *Nature*, 2014, **516**, 78–81.

12 Y.-X. Yu, *J. Phys. Chem. C*, 2016, **120**, 5288–5296.

13 Y. Zhang, Z. Mu, C. Yang, Z. Xu, S. Zhang, X. Zhang, Y. Li, J. Lai, Z. Sun, Y. Yang, Y. Chao, C. Li, X. Ge, W. Yang and S. Guo, *Adv. Funct. Mater.*, 2018, **28**, 1707578.

14 B. Ahmed, D. H. Anjum, Y. Gogotsi and H. N. Alshareef, *Nano Energy*, 2017, **34**, 249–256.

15 Q. Shan, X. Mu, M. Alhabeb, C. E. Shuck, D. Pang, X. Zhao, X.-F. Chu, Y. Wei, F. Du, G. Chen, Y. Gogotsi, Y. Gao and Y. Dall'Agnese, *Electrochem. Commun.*, 2018, **96**, 103–107.

16 M. W. Barsoum, *Prog. Solid State Chem.*, 2000, **28**, 201–281.

17 Q. Tao, M. Dahlqvist, J. Lu, S. Kota, R. Meshkian, J. Halim, J. Palisaitis, L. Hultman, M. W. Barsoum, P. O. Å. Persson and J. Rosen, *Nat. Commun.*, 2017, **8**, 14949.

18 R. Meshkian, M. Dahlqvist, J. Lu, B. Wickman, J. Halim, J. Thörnberg, Q. Tao, S. Li, S. Intikhab, J. Snyder, M. W. Barsoum, M. Yildizhan, J. Palisaitis, L. Hultman, P. O. Å. Persson and J. Rosen, *Adv. Mater.*, 2018, **30**, 1706409.

19 M. Dahlqvist, J. Lu, R. Meshkian, Q. Tao, L. Hultman and J. Rosen, *Sci. Adv.*, 2017, **3**, e1700642.

20 B. Ahmed, A. E. Ghazaly and J. Rosen, *Adv. Funct. Mater.*, 2020, **30**, 2000894.

21 M. Hu, H. Zhang, T. Hu, B. Fan, X. Wang and Z. Li, *Chem. Soc. Rev.*, 2020, **49**, 6666–6693.

22 L. Qin, Q. Tao, A. El Ghazaly, J. Fernandez-Rodriguez, P. O. Å. Persson, J. Rosen and F. Zhang, *Adv. Funct. Mater.*, 2018, **28**, 1703808.

23 A. S. Etman, J. Halim and J. Rosen, *Mater. Adv.*, 2021, **2**, 743–753.

24 Z. Ling, C. E. Ren, M.-Q. Zhao, J. Yang, J. M. Giammarco, J. Qiu, M. W. Barsoum and Y. Gogotsi, *Proc. Natl. Acad. Sci. U. S. A.*, 2014, **111**, 16676.

25 H. Xu, D. Zheng, F. Liu, W. Li and J. Lin, *J. Mater. Chem. A*, 2020, **8**, 5853–5858.

26 J. Yan, C. E. Ren, K. Maleski, C. B. Hatter, B. Anasori, P. Urbankowski, A. Sarycheva and Y. Gogotsi, *Adv. Funct. Mater.*, 2017, **27**, 1701264.

27 Q. Yang, Z. Xu, B. Fang, T. Huang, S. Cai, H. Chen, Y. Liu, K. Gopalsamy, W. Gao and C. Gao, *J. Mater. Chem. A*, 2017, **5**, 22113–22119.

28 M.-Q. Zhao, C. E. Ren, Z. Ling, M. R. Lukatskaya, C. Zhang, K. L. Van Aken, M. W. Barsoum and Y. Gogotsi, *Adv. Mater.*, 2015, **27**, 339–345.

29 Y. Li, Z. Yin, G. Ji, Z. Liang, Y. Xue, Y. Guo, J. Tian, X. Wang and H. Cui, *Appl. Catal., B*, 2019, **246**, 12–20.

30 N. H. Attanayake, S. C. Abeyweera, A. C. Thenuwara, B. Anasori, Y. Gogotsi, Y. Sun and D. R. Strongin, *J. Mater. Chem. A*, 2018, **6**, 16882–16889.

31 J. Li, B. Rui, W. Wei, P. Nie, L. Chang, Z. Le, M. Liu, H. Wang, L. Wang and X. Zhang, *J. Power Sources*, 2020, **449**, 227481.

32 L. Zhang, S. Yang, J. Chang, D. Zhao, J. Wang, C. Yang and B. Cao, *Front. Chem.*, 2020, **8**, 413.

33 H. Alnoor, A. Elsukova, J. Palisaitis, I. Persson, E. N. Tseng, J. Lu, L. Hultman and P. O. Å. Persson, *Mater. Today Adv.*, 2021, **9**, 100123.

34 J. Tang, X. Huang, T. Qiu, X. Peng, T. Wu, L. Wang, B. Luo and L. Wang, *Chem.–Eur. J.*, 2021, **27**, 1921–1940.

35 N. Joseph, P. M. Shafi and A. C. Bose, *Energy Fuels*, 2020, **34**, 6558–6597.

36 X. Wang, W. Ding, H. Li, H. Li, S. Zhu, X. Zhu, J. Dai, Z. Sheng, H. Wang, X. Zhu, Y. Sun and S. X. Dou, *J. Mater. Chem. A*, 2019, **7**, 19152–19160.